Local Conformational Changes Induced in B-DNA by Ethidium Intercalation†

James M. Benevides and George J. Thomas, Jr.*

School of Biological Sciences, University of Missouri—Kansas City, 5100 Rockhill Road, Kansas City, Missouri 64110-2499

Received June 28, 2004; Revised Manuscript Received October 19, 2004

ABSTRACT: Structural effects of binding the intercalating drug ethidium bromide (EtBr) to 160 base pair (bp) fragments of nucleosomal calf thymus DNA have been probed by the method of Raman difference spectroscopy. With the use of a near-infrared (NIR) laser source to excite the Raman spectrum at 752 nm, vibrational signatures of both the EtBr intercalant and DNA target have been identified in spectra of the drug−DNA complexes. Analysis of the results obtained on complexes consisting of 1 EtBr bound/10 bp leads to the following conclusions: (i) Raman markers diagnostic of DNA phosphodiester conformation are converted from the B type to the A type with EtBr binding, commensurate with the proportion of ethidium-bound nucleotides in the complex. (ii) Ethidium binding converts deoxynucleoside sugar puckers from the C2′-endo to the C3′-endo conformation, also consistent with binding stoichiometry. Both pyrimidine and purine deoxynucleoside sugar puckers are perturbed by the phenanthridinium ring intercalation. (iii) Phenanthridinium insertion between bases is accomplished with no apparent change in hypochromicities of purine or pyrimidine Raman markers, indicating that base−phenanthridinium interactions provide compensatory hypochromic effects. (iv) Novel Raman markers of helix unwinding have been identified and assigned primarily to methylene deformation modes of the deoxyribosyl C2′H_2 and C5′H_2 groups. The present study provides new insights into drug−DNA recognition in solution and demonstrates the feasibility of NIR−Raman spectroscopy for structural studies of highly chromophoric DNA complexes.

A goal of drug-based therapy is the targeting of a ligand to DNA to alter genome structure and function with high specificity. Rational drug design thus requires detailed knowledge of both the binding characteristics of the drug and the structural consequences of ligation. Ideally, such information is required for DNA targets of genomic size and complexity. While thermodynamic and kinetic properties have been assayed for a wide range of drugs and DNA targets (*1*−*3*), structural studies have been limited almost exclusively to drug ligation by small oligonucleotides (*4*−*14*).

Raman spectroscopy has the potential to probe structural details of solution complexes between drugs and DNA molecules of genomic size and topological diversity. Typical of DNA-intercalating drugs is ethidium bromide (EtBr),[1] a phenanthridinium compound (Figure 1) for which considerable DNA binding data have been reported (*15*−*17*). Unfortunately, conventional Raman analysis of ethidium and its DNA complexes by use of laser excitation wavelengths in the visible region is not feasible owing to the prohibitively intense fluorescence of the phenanthridinium moiety throughout much of the 400−600 nm interval. Although fluorescence interference could be circumvented in principle by use of Fourier transform (FT) Raman spectroscopy via 1064-nm excitation, the FT-Raman approach suffers from very low spectral sensitivity. Similarly, the FTIR method is disadvantaged vis-à-vis Raman by the very high opacity of water to infrared radiation. Finally, we note that the method of ultraviolet-resonance Raman (UVRR) spectroscopy of drug−DNA complexes is also limited—in this case by the fact that UV laser excitation wavelengths below 400 nm preclude the possibility of gaining direct structural information about the DNA backbone (*18*).

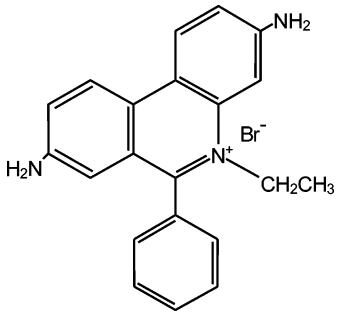

FIGURE 1: Structural formula of ethidium bromide (EtBr).

We have overcome all of the foregoing limitations and succeeded in obtaining Raman spectra of both ethidium-free and ethidium-bound DNA using the near-infrared (NIR) laser excitation wavelength of 752 nm and a Raman spectrometer system designed for optimum performance in the NIR region. NIR excitation of the Raman spectrum not only circumvents ethidium fluorescence but also has the potential to simultaneously probe both the drug and DNA components of a complex. NIR−Raman spectroscopy of ethidium/DNA is therefore expected to reveal structural features of the DNA

† Paper LXXXIV in the series Raman Spectral Studies of Nucleic Acids. Supported by National Institutes of Health Grant GM54378.

* To whom correspondence should be addressed: telephone 816-235-5247; fax 816-235-1503; e-mail thomasgj@umkc.edu.

[1] Abbreviations: ds, double-stranded; bp, base pair; DNA^{160bp}, 160-bp mononucleosomal calf thymus DNA; EtBr, ethidium bromide; EtBr/DNA, complex of ethidium bromide and DNA; NIR, near-infrared; UVRR, ultraviolet resonance Raman.

10.1021/bi048651l CCC: $30.25 © 2005 American Chemical Society
Published on Web 02/04/2005

phosphodiester backbone as well as those of the base and phenanthridinium residues (*19*−*23*).

Much of our understanding of the structural details of ethidium-bound nucleic acids is derived from X-ray analyses of crystalline complexes of EtBr with various diribonucleoside monophosphates (*4*, *5*). A consequence of phenanthridinium intercalation in these RNA fragments, irrespective of the base sequence, is C2′-endo puckering of the 5′-ribosyl moiety and C3′-endo puckering of the 3′-ribosyl moiety. Such mixed sugar puckering may facilitate the increased interbase separation (6.7 Å) and reduced winding angle (8−10°) that are imposed by phenanthridinium intercalation (*24*, *25*). Crystallography of the EtBr/ribodinucleotide complexes indicates that the phenyl and ethyl groups of ethidium are positioned in what would represent the minor groove of an extended nucleic acid duplex, while the positive charge of the phenanthridinium moiety (Figure 1) is situated so as to provide favorable electrostatic interaction with the nucleotide phosphate. Hydrogen bonding between phenanthridinium and RNA (or DNA) sites is not suggested by the crystal structures. The absence of such hydrogen bonds is presumed to distinguish ethidium from other more complex nucleic acid intercalators (*6*).

In addition to offering the prospect of new insights into structural consequences of ethidium intercalation, Raman spectroscopy of EtBr/DNA complexes is expected to complement ongoing Raman studies of protein−DNA recognition (*20*, *21*, *23*). For example, the unwinding of double-stranded B-DNA that is induced by phenanthridinium intercalation (*24*, *25*) can also be promoted by DNA-binding proteins (*26*, *27*). Such ligand-induced unwinding is expected to significantly perturb well-characterized Raman markers of B-DNA (*21*−*23*). Raman band perturbations specific to DNA helix unwinding have been difficult to assess from studies of protein−DNA complexes because the protein-induced unwinding also generates a myriad of other local structural perturbations in B-DNA, including bending and kinking of the double helix (*28*−*30*). Accordingly, the present study is expected to provide an alternative approach for evaluating how changes in the helix winding angle may affect the Raman signature of B-DNA.

In this work we show that ethidium intercalation of B-DNA in the EtBr/DNA complex causes pronounced changes to the Raman signatures of both the EtBr and DNA components. To delineate spectral perturbations, we have examined both H_2O and D_2O solutions of the EtBr/DNA complexes and exploited the fact that qualitatively and quantitatively different deuteration shifts are observed for the EtBr and DNA constituents. We have found that changes in Raman markers of the DNA backbone which result from ethidium intercalation provide an interesting complement to those reported previously for other DNA structural transitions (*31*−*33*).

MATERIALS AND METHODS

Mononucleosomal 160-bp DNA was prepared by digesting high-molecular-weight calf thymus DNA (Amersham Pharmacia) by standard methods (*34*). Electrophoresis-grade ethidium bromide (EtBr) was purchased from Fisher Scientific. Oligonucleotide duplexes [$d(GC)_6$ and $d(AT)_{10}$] were purchased from Sigma-Genosys (The Woodlands, TX). H_2O and D_2O solutions of DNA or oligonucleotides (25 mg/mL), EtBr (1.6 mg/mL), and their complexes were prepared containing 100 mM NaCl and adjusted to neutrality (pH or pD 7) by addition of dilute NaOH or NaOD. Spectral data shown below were obtained primarily from complexes containing one EtBr molecule/10 bp in the DNA target.

For Raman measurements, aliquots of solutions of EtBr, DNA, and 1:5 and 1:10 complexes were sealed in glass capillaries. Raman spectra were collected on a Kaiser Optical HoloSpec VPT spectrometer (Ann Arbor, MI) equipped with a liquid-nitrogen-cooled, charge-coupled device detector optimized for the near-infrared region (Roper, model 1024EHRB, Trenton, NJ). Spectra were excited at 752 nm with ∼150 mW of radiant power from a titanium/sapphire laser (Coherent, model 890, Palo Alto, CA), which was pumped at 532 nm (Spectra-Physics, model Millennia X, Mountain View, CA). Each spectrum displayed in the figures is the average of 140 exposures of 15 s each. Raman wavenumbers were calibrated by use of the emission lines from a neon lamp and the 459 cm^{-1} band of liquid CCl_4. Weak scattering by the aqueous solvent was removed by established computer subtraction techniques (*35*). Raman markers of the DNA phosphate group (1092 cm^{-1}) and EtBr phenyl ring (1001 cm^{-1}) were employed for spectral intensity normalizations, as also described previously (*31*, *36*).

Complexes of the desired stoichiometry (e.g., 1 EtBr/10 bp of DNA) were prepared by use of the known molar extinction coefficients of EtBr ($\epsilon_{480} = 5860\ M^{-1}\ cm^{-1}$) and DNA ($\epsilon_{260} = 6600\ M^{-1}\ cm^{-1}$). The Raman difference spectrum between complex and sum-of-constituents was computed (*20*) by compensating the marker bands serving as intensity standards for DNA (1092 cm^{-1}) and EtBr (1001 cm^{-1}). In this protocol, the sum-of-constituents spectrum is generated by direct addition of the component spectra (EtBr and DNA), weighted appropriately to ensure no residual difference intensity at either 1092 or 1001 cm^{-1} in the subsequently computed digital difference spectrum. Typically, only a few iterations were required to achieve the correct weighting.

RESULTS

1. NIR−Raman Spectrum of Ethidium Bromide. The 752-nm excited Raman spectrum of ethidium bromide (EtBr) in H_2O solution is shown in trace A of Figure 2. The 450−1750 cm^{-1} interval of this spectrum, which is rich in Raman bands due to localized vibrations of the phenanthridinium, phenyl, and ethyl moieties, represents the first reported Raman signature of an ethidium compound. A Raman spectrum of similar quality, also with 752-nm excitation, has been obtained for the D_2O solution of EtBr (not shown in Figure 2 but available as Supporting Information). Preliminary assignments for the Raman bands of EtBr, based upon the H_2O and D_2O solution spectra and additional Raman data from model compounds, are given in Table 1. More detailed assignments for selected vibrational modes of the phenanthridinium ring have also been discussed elsewhere (*37*).

2. NIR−Raman Spectra of DNA and Ethidium-DNA Complexes. The 752-nm excited Raman spectrum of 160-bp DNA in H_2O solution is shown in trace C of Figure 2. This spectrum exhibits all of the Raman bands diagnostic of B-DNA (*31*, *38*−*41*). As expected, however, the band

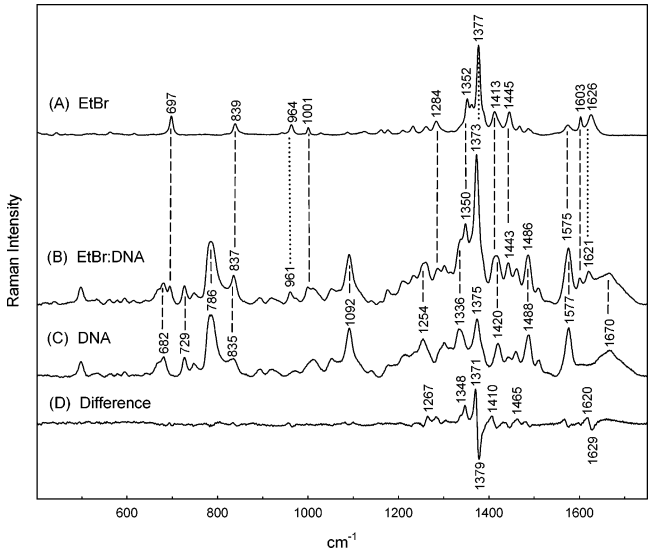

FIGURE 2: Raman spectra (450−1750 cm^{-1}) of solutions of EtBr at 1.6 mg/mL (trace A), 160-bp DNA at 20 mg/mL (trace C), and the EtBr/DNA complex (trace B) at 20 mg/mL. The complex contains 1 EtBr ligand/10 base pairs (bp). Spectra were excited at 752 nm and corrected for contributions from the aqueous solvent (100 mM NaCl, pH 7.0, 20 °C). Also shown is the computed Raman difference spectrum (trace D) obtained by subtracting the spectral sum (trace A + trace C) from the spectrum of the complex (trace B). The difference spectrum shows to scale the magnitudes of Raman band shifts and intensity changes resulting from ethidium−DNA interaction. Vertical broken lines connect key marker bands in spectra of EtBr and DNA to their counterparts in the spectrum of the complex; dotted lines connect bands of EtBr or DNA that are shifted significantly in the complex.

intensities for 752-nm excitation are markedly different than those reported previously for 488-, 514-, and 532-nm excitations. A tabulation of the Raman band assignments and relative Raman intensities observed for 752- and 532-nm excitations of the DNA spectrum is given in Table 2. Further discussion of the Raman band assignments of B-DNA has been given elsewhere (*19*).

Trace B of Figure 2 shows the Raman spectrum of a complex of EtBr with 160-bp DNA, obtained by titrating the DNA with EtBr up to a molar ratio of 1 ethidium/10 base pairs (1:10 EtBr/DNA). At this stoichiometry, virtually all of the ethidium is bound to DNA whereas no more than 20% of the DNA bases can be affected (*42*). Although Raman bands of both EtBr and DNA contribute prominently to the spectrum of the complex—as indicated in Figure 2 by the vertical lines interconnecting prominent bands of the complex with those of the constituents—the binding stoichiometry employed here implies that Raman bands of EtBr will be more affected than those of DNA.

Trace D of Figure 2 illustrates the prolific Raman difference spectrum obtained by subtracting from the spectrum of the EtBr/DNA complex (trace B) the spectral sum of its EtBr (trace A) and 160-bp DNA (trace C) constituents, demonstrating that complex formation leads to extensive perturbations of localized vibrational modes of the interacting drug and DNA molecules. The largest spectral perturbations are evident for phenanthridinium Raman markers in the 1350−1400 cm^{-1} interval, although significant perturbations are also observed for DNA Raman markers in the 600−850 and 1400−1600 cm^{-1} intervals. Interpretation of these results in terms of the interacting molecular sites is facilitated by consideration of complementary data from corresponding D_2O solutions (Figure 3). Analogous approaches have been used previously to facilitate interpretation of DNA conformational transitions (*32*, *43*) and protein−DNA interactions (*44*).

Table 1: Raman Frequencies,[a] Intensities, and Assignments for Ethidium Bromide

H_2O solution		D_2O solution		
frequency (cm^{-1})	relative intensity	frequency (cm^{-1})	relative intensity	assignment[b]
519b	0.2	512	0.2	
562	0.4	560	0.4	
		590	0.2	ND_2 def (wag?)
615	0.3	617	0.3	phenyl ring
654	0.1	648	0.2	
697	2.2	692	1.8	phenanthridinium ring
821s	0.2			NH_2 def (wag?)
839	1.3	829	1.6	phenanthridinium ring
943	0.3	950s	0.2	
964	1.2	971	1.1	
1001	0.9	1001	0.9	phenyl ring
1012s	1.6			C−N str
1029	0.3	1030	0.2	phenyl ring
1088	0.4	1088	0.3	C−C, C−N str
1119s	0.4			C−C, C−N str
1125b	0.5	1125	0.5	C−C, C−N str
1162	0.7			C−C, C−N str
1156	1.3			ND_2 def (scissor?)
1177	0.6	1179	0.9	phenyl ring
1198s	0.4			C−C, C−N str
1210	0.6	1210	0.8	phenyl ring
1233	1.0	1243	0.4	CH def
1261	1.0	1276s	1.4	CH def
1284	1.6	1288	2.2	CH def
1317b	0.5			phenanthridinium ring
1352	1.4	1344s	2.8	phenanthridinium ring
1362s	3.5	1357s	3.4	phenanthridinium ring
1377	10.0	1369	10	phenanthridinium ring
1386s	3.0	1389s	1.7	CH_3 def
1413	2.7	1411	4.0	phenanthridinium ring
1445	2.6	1440	3.0	CH_2 def
1468	1.0	1461	1.7	CH_3 def
1487	0.8	1486	0.5	phenanthridinium ring
		1549s	0.4	
1575	1.2	1573	1.2	phenanthridinium ring
1603	2.0	1603	2.3	phenyl ring
1626	2.3	1629	4.2	NH_2 sci; phenanthridinium ring
2884	nd	nd	nd	al CH str
2945	nd	nd	nd	al CH str
3002	nd	nd	nd	ar CH str

[a] Frequencies are in wavenumber (cm^{-1}) units; and relative intensities are on an arbitrary 0−10 scale. [b] Abbreviations: b, broad band; s, shoulder; def, deformation; str, stretch; sci, scissor; al, aliphatic; ar, aromatic; nd, not determined.

Figure 3 compares the Raman difference spectrum of the H_2O solution of the EtBr/DNA complex with its D_2O solution counterpart (top trace) and also with difference spectra for model oligodeoxynucleotide/EtBr complexes (bottom two traces). Here, the ordinates for the intervals 600−900 cm^{-1} (left panel) and 1250−1750 cm^{-1} (right panel) have been appropriately scaled to accommodate the greater magnitude of perturbations suffered by EtBr markers of the latter interval.

DISCUSSION

Raman spectroscopy has been exploited previously as a conformational probe of genomic DNA complexes in aqueous solutions and condensed states (*38*, *41*, *45*−*49*). Here, we extend the method by use of near-infrared laser excitation to solutions of the highly chromophoric complex formed between the intercalating drug ethidium bromide (EtBr) and monodisperse nucleosomal calf thymus DNA fragments of 160 bp.

Table 2: Raman Band Frequencies and Intensities of Nucleosomal Calf Thymus DNA (160 bp) Obtained with 752- and 532-nm Excitations[a]

752 nm		532 nm		
frequency (cm^{-1})	relative intensity	frequency (cm^{-1})	relative intensity	assignment[b]
415	0.8	412	0.9	
432	0.7	437	0.6	
452	0.6			
472	0.7			
490s	1.0			
501	2.8	497	2.0	G, T
534	0.7	532	0.6	A
567	0.6	562	0.5	T
583	0.5	578	0.6	
596	0.8	594	1.0	C, G
626	0.4			
646	0.8	642	0.6	A, C
670	2.4	670	2.5	T
682	3.3	681	3.4	G
729	3.8	727	3.5	A
750	2.6	748	2.3	T
784	10.0	785	10.0	C
788s	9.9			bk (OPO str)
835	2.9	834	2.9	bk (OPO str)
894	1.3	894	1.6	bk
917	1.1	919	1.2	bk
925	1.0			bk
970	0.9	971	0.5	bk
		994	1.2	bk
1011	2.7	1013	2.2	T
1053	3.0	1052	2.2	bk (CO str)
1067	2.6	1070	2.1	bk (CO str)
1092	8.2	1092	8.2	bk (PO_2^- str)
1107s	3.2			bk
1142	1.2	1142	0.9	T
1175	2.0	1177	1.8	T
1190	2.0	1191	1.5	bk
1212	3.5	1214	3.2	T, A
1237	3.8	1237	1.1	T
1254	5.7	1255	5.1	C, A, T
1292s	3.8	1292s	4.1	C
1301	4.8	1302	5.2	A, T
1318	3.8	1315	3.8	G
1336	6.7	1337	7.1	A, G
1375	8.2	1374	8.8	T, G, A
1385s	3.5			
1420	4.1	1420	3.1	A, bk (C5′H_2 def)
1443	2.1	1443	1.1	bk (C5′H_2 def)
1460	3.4	1461	2.1	bk (C2′H_2 def)
1488	6.6	1488	8.8	G, A, T
1510	2.7	1510	1.9	A, C
1532	0.7	1528	0.4	C, G
1577	7.5	1577	7.6	G, A
		1600	1.6	C
1647	3.8	1650	3.3	T (C4=O/C5=C6 str), C
1670	5.8	1668	4.6	T (C4=O/C5=C6 str)
1686s	4.7	1693	2.9	T (C2=O str)
1716s	2.4	1715	1.7	G (C6=O str)

[a] Frequencies are in wavenumber (cm^{-1}) units and relative intensities are on an arbitrary 0−10 scale, with 10 assigned to the most intense band (784 cm^{-1}) in each spectrum; s indicates a partially resolved shoulder. [b] A, T, G, C, and bk indicate bands assigned to base ring vibrations and the DNA backbone, respectively. Other abbreviations: str, stretch; def, deformation. More specific bond vibrational assignments, when known, are given in parentheses. (See also refs *48*, *55*, and *56*.)

1. Raman Fingerprint of Ethidium−DNA Interaction. The difference spectrum computed by subtracting the sum of Raman spectra of DNA and EtBr constituents from the Raman spectrum of their EtBr/DNA complex represents a Raman fingerprint of ethidium−DNA interaction. Examples of such fingerprints are shown in Figure 3 for complexes of EtBr with $d(AT)_{10}$, $d(GC)_6$, and 160-bp calf thymus nucleosomal DNA. The 1200−1700 cm^{-1} interval of each fingerprint of Figure 3 exhibits many prominent features (peaks at 1267, 1285, and 1348 cm^{-1} and peak/trough couplets at 1371/1379 and 1620/1629 cm^{-1}) that are independent of the base composition of the DNA target. Accordingly, these difference features also represent a fingerprint of phenanthridinium intercalation, irrespective of the target base sequence. The peak/trough couplets at 838/844, 1410/1420, 1436/1448, and 1465/1475 cm^{-1}, which are also common to the three complexes, are likewise assigned primarily to the intercalated drug. Although weaker overlapping Raman bands of DNA may be present (Table 2), assignment primarily to intercalated EtBr is justified by the fact that the observed deuteration shifts (cf. top two traces of Figure 3) parallel those observed upon deuteration of the free drug (Table 1).

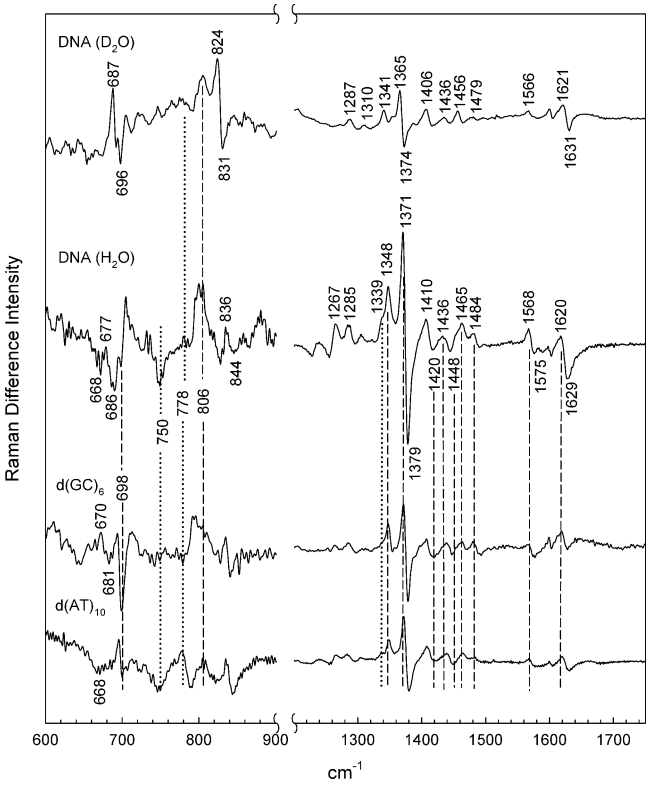

FIGURE 3: From top to bottom: Raman difference signatures (600−900 and 1200−1750 cm^{-1} regions) of the 1:5 EtBr/DNA complex in D_2O and H_2O solutions and corresponding 1:10 complexes of EtBr with model oligodeoxynucleotides containing only GC pairs [EtBr/$d(GC)_6$] and only AT pairs [EtBr/$d(AT)_{10}$]. The ordinate scale of the 600−900 cm^{-1} spectral interval is expanded 8-fold in relation to the accompanying 1200−1750 cm^{-1} interval. The dashed lines connect difference features that are common to all the complexes; dotted lines connect difference features that are base-composition-dependent. Experimental conditions are as given in Figure 2.

The 600−900 cm^{-1} interval of Figure 3 also reveals Raman difference features between each of the three EtBr/DNA complexes and its constituents. However, because the ordinate scale for this interval of the spectrum has been expanded 8-fold in relation to the accompanying 1200−1700 cm^{-1} interval, these difference features are relatively small by comparison. With the possible exception of the sharp troughs and peaks between 690 and 700 cm^{-1}, all of the difference features of the 600−900 cm^{-1} interval are assignable to DNA (Table 2) and all appear to be dependent in detail upon the base sequence. We note, for example, that the 806 cm^{-1} difference feature occurs as a dominant peak

in 160-bp DNA but as a lesser peak in $d(AT)_{10}$ and as an obscure shoulder in $d(GC)_6$. Accordingly, this interval of the difference spectrum is proposed as a fingerprint of nucleotide-specific structural perturbations induced by EtBr at its particular binding sites, as discussed in the following section.

2. DNA Structural Perturbations: (a) Deoxyribosyl Conformation. Ethidium-intercalated sites in crystal structures of ribodinucleoside monophosphate complexes are characterized by C3′-endo and C2′-endo puckering for the 3′- and 5′-ribosyl moieties, respectively, in lieu of the exclusively C3′-endo puckering observed in the absence of bound ethidium. The mixed sugar conformations of the complex presumably accommodate the low helix winding angle ($\Omega \sim 10°$) and large base pair separation ($D_z = 6.7$ Å) resulting from ethidium insertion (*7*). In such complexes, ethidium has been described as a *simple* intercalator, engaged in stacking interactions with the bases and electrostatic interactions with the oppositely charged sugar−phosphate backbone. Conversely, *complex* intercalators are distinguished by a normal helix winding angle ($\Omega \sim 36°$) and exclusively C3′-endo ribosyl puckering. Although no crystal structure is available for any oligodeoxynucleotide complex of EtBr, it has been proposed that the simple and complex intercalation models apply also to DNA models (*7*). Because both simple and complex intercalations are characterized by C3′-endo puckering at the intercalation sites (though in different amounts), it is of interest to assess whether such C3′-endo puckering is evidenced by Raman markers of the EtBr/DNA complexes examined here.

Raman bands of DNA that are potentially informative of deoxyribosyl pucker (and glycosyl bond torsion angle) occur in the interval 600−900 cm^{-1} (*19*, *50*). Those of dT and dG have been particularly useful in previous studies (*51*−*54*). For example, the C2′-endo/anti dT conformation of B-DNA has a Raman marker at 750 cm^{-1}, which undergoes an approximate 50% loss of intensity upon changing to the C3′-endo/anti dT conformation of *A* DNA (*32*). Similarly, the C2′-endo/anti dG conformation has a Raman marker at 682 cm^{-1}, which shifts to approximately 664 cm^{-1} for the C3′-endo/anti dG conformation (*52*).

Interestingly, the Raman difference signature of EtBr/$d(AT)_{10}$ (Figure 3, bottom trace) exhibits a trough at 750 cm^{-1}, consistent with a conversion of dT moieties from C2′-endo/anti to C3′-endo/anti. Based upon Raman studies of the B-DNA → A-DNA transition (*32*), the observed trough intensity corresponds to pucker conversion by 15% ± 7% of deoxynucleoside residues, where the limit error reflects the spectral noise level. Although the precision of the results is not sufficient to distinguish between models of simple (10% conversion expected) and complex intercalation (20% conversion), the Raman spectrum identifies intercalant-induced dT conformational change in the solution complex of EtBr/$d(AT)_{10}$. A 750 cm^{-1} trough corresponding to 15% ± 8% dT pucker conversion is also revealed in the Raman difference signature of the EtBr/DNA complex (Figure 3, second trace from top). As expected, this type of difference feature is absent from the EtBr/$d(GC)_6$ complex.

In the case of EtBr/$d(GC)_6$ we observe a trough at 681 cm^{-1} and peak at 670 cm^{-1} (Figure 3, second trace from bottom), which are features consistent with a conversion of dG moieties from C2′-endo/anti to C3′-endo/anti. Again, based upon the B-DNA → A-DNA studies (*52*), the results suggest 15% ± 8% pucker conversion. Similar shifting of dG conformational markers occurs in the EtBr/DNA complex (Figure 3, second trace from top).

The data of Figure 3 indicate that ethidium intercalation in DNA of mixed base composition drives deoxynucleosides of both pyrimidines and purines from C2′-endo to C3′-endo sugar pucker.

(b) Phosphodiester Conformation. A positive difference feature is observed near 806 cm^{-1} in all difference spectra displayed in Figure 3. This Raman difference band most likely arises from a conformational rearrangement of phosphodiester torsion angles of the DNA backbone in the complex. Consistent with this assignment is the persistence of the difference feature in the deuterated complex (Figure 3, top trace). A Raman band near 806 cm^{-1} has been assigned previously as a Raman marker diagnostic of A-DNA (*32*). The combination of an 806 cm^{-1} band and C3′-endo/anti nucleoside conformers is compatible with ethidium-induced transformation of the DNA backbone from the B form to the A form at the sites of intercalation. Additional band shifts, 788 → 779 and 1420 → 1410 cm^{-1}, are reminiscent of those reported earlier for the B → A transformation of poly(dA-dT)·poly(dA-dT) (*32*).

(c) Base Stacking. Phenanthridinium intercalation in the EtBr/DNA complex approximately doubles the vertical separation of the bases (D_z) to 6.7 Å (*4*). Because this results in no change of Raman hypochromism for the well-characterized and sensitive base-stacking markers of dA and dT near 728 and 1238 cm^{-1}, respectively (*55*, *56*), we conclude that base−phenanthridinium stacking effectively compensates for the eliminated base−base stacking interactions.

(d) Helix Unwinding. Phenanthridinium intercalation in EtBr/DNA complexes reduces the helix winding angle (Ω) of B-DNA from 36° to approximately 10° (*12*−*14*). To assess whether Raman markers of helix unwinding could be identified in the difference spectrum of the EtBr/DNA complex (Figure 3), the present results have been compared with Raman difference signatures of other DNA structure transformations (*19*) and protein/DNA complex formations (*23*, *57*). For example, helix unwinding that accompanies the binding of architectural proteins to B-DNA is known to perturb Raman indicators of backbone geometry in the 1410−1470 cm^{-1} interval (*21*−*23*). Similar Raman band perturbations also accompany the B → A transformations of DNA (*31*, *39*, *58*) and polynucleotides (*32*, *58*). The affected Raman markers, which are assignable primarily to methylene deformation modes of the deoxyribosyl $C2'H_2$ and $C5'H_2$ groups (Table 2), are significantly perturbed by EtBr binding to B-DNA (Figure 3). Accordingly, we attribute the pattern of peaks and troughs in the 1410−1470 cm^{-1} interval in the difference spectra of Figure 3 to phenanthridinium-induced helix unwinding and accompanying changes (C2′-endo → C3′-endo) in deoxyribosyl ring pucker. A very similar difference signature is also observed in the D_2O solution spectrum (Figure 3, top trace).

(e) Other. Hydrogen-bonding interactions between exocyclic substituents of the bound drug and the phosphate oxygens of DNA may also stabilize the intercalative geometry of simple intercalators such as EtBr. However, these are not expected to produce large spectral perturbations to

Raman markers of either the drug (EtBr) or its target (DNA), and no difference bands are so assigned in Figure 3.

CONCLUSIONS

Raman spectra of complexes formed between ethidium bromide and 160-bp DNA with drug/base pair stoichiometries of 1:10 and 1:5 have been successfully obtained for the near-infrared laser excitation wavelength of 752 nm. Structural markers of both the drug and DNA moieties have been identified in the spectra and assigned to localized vibrational modes of interacting groups. Comparison of the Raman signature of each complex with corresponding signatures of its drug and DNA constituents indicates that phenanthridinium intercalation at ~10% of base sites drives approximately 10−20% of DNA deoxynucleosides from C2′-endo pucker (B-type conformation) to C3′-endo pucker (A-type conformation). Both pyrimidine and purine deoxynucleosides are affected. The results obtained here thus extend earlier findings (*12*−*14*), which identified changes only in the puckering of purine deoxynuclosides.

Raman spectra of EtBr/DNA complexes also extend earlier findings on key Raman markers of nucleic acid backbone conformation (*58*, *59*). Thus, drug-intercalated DNA exhibits a Raman marker near 806 cm^{-1}, which is analogous to the Raman markers observed near 805−815 cm^{-1} in spectra of RNA (*59*, *60*), deformed DNA (*61*, *62*), and many nucleoproteins (*23*, *63*, *64*). In all cases, the Raman marker is diagnostic of the C3′-endo sugar conformation, which is absent from canonical B-DNA and other nucleic acids containing only C2′-endo sugars. Ethidium-induced shifts of B-DNA Raman markers at 680, 750, 790, 1420, 1445, and 1460 cm^{-1} have also been identified with phenanthridinium intercalation and may reflect structural perturbations to either the backbone or base environments of the DNA target.

Finally, the present study demonstrates the effectiveness of NIR−Raman spectroscopy as a structural probe of highly fluorescent DNA complexes.

SUPPORTING INFORMATION AVAILABLE

Figures comparing NIR−Raman spectra of EtBr in H_2O and D_2O solutions (Figure S1) and showing the original data used to generate the difference traces of Figure 3 (Figure S2). This material is available free of charge via the Internet at http://pubs.acs.org.

REFERENCES

1. Haq, I., and Ladbury, J. (2000) Drug−DNA recognition: energetics and implications for design, *J. Mol. Recognit. 13*, 188−197.
2. Han, X., and Gao, X. (2001) Sequence specific recognition of ligand−DNA complexes studied by NMR, *Curr. Med. Chem. 8*, 551−581.
3. Haq, I. (2002) Thermodynamics of drug−DNA interactions, *Arch. Biochem. Biophys. 403*, 1−15.
4. Jain, S. C., and Sobell, H. M. (1984) Visualization of drug−nucleic acid interactions at atomic resolution. VIII. Structures of two ethidium/dinucleoside monophosphate crystalline complexes containing ethidium:cytidylyl(3′-5′) guanosine, *J. Biomol. Struct. Dyn. 1*, 1179−1194.
5. Jain, S. C., and Sobell, H. M. (1984) Visualization of drug−nucleic acid interactions at atomic resolution. VII. Structure of an ethidium/dinucleoside monophosphate crystalline complex, ethidium: uridylyl(3′-5′) adenosine, *J. Biomol. Struct. Dyn. 1*, 1161−1177.
6. Sakore, T. D., Bhandary, K. K., and Sobell, H. M. (1984) Visualization of drug−nucleic acid interactions at atomic resolution. X. Structure of a *N,N*-dimethylproflavine:deoxycytidylyl-(3′-5′)deoxyguanosine crystalline complex, *J. Biomol. Struct. Dyn. 1*, 1219−1227.
7. Bhandary, K. K., Sakore, T. D., Sobell, H. M., King, D., and Gabbay, E. J. (1984) Visualization of drug−nucleic acid interactions at atomic resolution. IX. Structures of two *N,N*-dimethylproflavine:5-iodocytidylyl (3′-5′) guanosine crystalline complexes, *J. Biomol. Struct. Dyn. 1*, 1195−1217.
8. Lybrand, T., and Kollman, P. (1985) Molecular mechanical calculations on the interaction of ethidium cation with double-helical DNA, *Biopolymers 24*, 1863−1879.
9. Moravek, Z., Neidle, S., and Schneider, B. (2002) Protein and drug interactions in the minor groove of DNA, *Nucleic Acids Res. 30*, 1182−1191.
10. Patel, D. J. (1997) Structural analysis of nucleic acid aptamers, *Curr. Opin. Chem. Biol. 1*, 32−46.
11. Feigon, J., Leupin, W., Denny, W. A., and Kearns, D. R. (1982) Binding of ethidium derivatives to natural DNA: a 300 MHz ^1H NMR study, *Nucleic Acids Res. 10*, 749−762.
12. Davies, D. B., Karawajew, L., and Veselkov, A. N. (1996) ^1H NMR structural analysis of ethidium bromide complexation with self-complementary deoxytetranucleotides 5′-d(ApCpGpT), 5′-d(ApGpCpT), and 5′-d(TpGpCpA) in aqueous solution, *Biopolymers 38*, 745−757.
13. Davies, D. B., Djimant, L. N., Baranovsky, S. F., and Veselkov, A. N. (1997) ^1H NMR determination of the thermodynamics of drug complexation with single-stranded and double-stranded oligonucleotides in solution: ethidium bromide complexation with the deoxytetranucleotides 5′-d(ApCpGpT), 5′-d(ApGpCpT), and 5′-d(TpGpCpA), *Biopolymers 42*, 285−295.
14. Davies, D. B., Pahomov, V. I., and Veselkov, A. N. (1997) NMR determination of the conformational and drug binding properties of the DNA heptamer d(GpCpGpApApGpC) in aqueous solution, *Nucleic Acids Res. 25*, 4523−4531.
15. Ren, J., and Chaires, J. B. (1999) Sequence and structural selectivity of nucleic acid binding ligands, *Biochemistry 38*, 16067−16075.
16. Ren, J., Jenkins, T. C., and Chaires, J. B. (2000) Energetics of DNA intercalation reactions, *Biochemistry 39*, 8439−8447.
17. Chaires, J. B. (2001) Analysis and interpretation of ligand−DNA binding isotherms, *Methods Enzymol. 340*, 3−22.
18. Lu, D. S., Nonaka, Y., Tsuboi, M., and Nakamoto, K. (1990) Molecular distortion of distamycin on binding to DNA as revealed by Raman spectroscopy, *J. Raman Spectrosc. 21*, 321−326.
19. Thomas, G. J., Jr., and Tsuboi, M. (1993) Raman spectroscopy of nucleic acids and their complexes, in *Advances in Biophysical Chemistry* (Bush, C. A., Ed.) Vol. 3, pp 1−70, JAI Press Inc., Greenwich, CT.
20. Benevides, J. M., Chan, G., Lu, X. J., Olson, W. K., Weiss, M. A., and Thomas, G. J., Jr. (2000) Protein-directed DNA structure. I. Raman spectroscopy of a high-mobility-group box with application to human sex reversal, *Biochemistry 39*, 537−547.
21. Benevides, J. M., Li, T., Lu, X. J., Srinivasan, A. R., Olson, W. K., Weiss, M. A., and Thomas, G. J., Jr. (2000) Protein-directed DNA structure II. Raman spectroscopy of a leucine zipper bZIP complex, *Biochemistry 39*, 548−556.
22. Benevides, J. M., and Thomas, G. J., Jr. (2002) DNA unwinding: analysis by near-infrared Raman spectroscopy of ethidium−DNA complexes. *Biophys. J. 82*, 125d.
23. Serban, D., Benevides, J. M., and Thomas, G. J., Jr. (2003) HU protein employs similar mechanisms of minor-groove recognition in binding to different B-DNA sites: demonstration by Raman spectroscopy, *Biochemistry 42*, 7390−7399.
24. Wang, J. C. (1974) The degree of unwinding of the DNA helix by ethidium. I. Titration of twisted PM2 DNA molecules in alkaline cesium chloride density gradients, *J. Mol. Biol. 89*, 783−801.
25. Liu, L. F., and Wang, J. C. (1975) On the degree of unwinding of the DNA helix by ethidium. II. Studies by electron microscopy, *Biochim. Biophys. Acta 395*, 401−412.
26. Wang, J. C., Barkley, M. D., and Bourgeois, S. (1974) Measurements of unwinding of lac operator by repressor, *Nature 251*, 247−249.
27. Werner, M. H., Huth, J. R., Gronenborn, A. M., and Clore, G. M. (1995) Molecular basis of human 46X,Y sex reversal revealed from the three-dimensional solution structure of the human SRY−DNA complex, *Cell 81*, 705−714.
28. Giese, K., Pagel, J., and Grosschedl, R. (1997) Functional analysis of DNA bending and unwinding by the high mobility group domain of LEF-1, *Proc. Natl. Acad. Sci. U.S.A. 94*, 12845−12850.

29. Dhavan, G. M., Crothers, D. M., Chance, M. R., and Brenowitz, M. (2002) Concerted binding and bending of DNA by *Escherichia coli* integration host factor, *J. Mol. Biol. 315*, 1027−1037.
30. Rice, P. A., Yang, S., Mizuuchi, K., and Nash, H. A. (1996) Crystal structure of an IHF−DNA complex: a protein-induced DNA U-turn, *Cell 87*, 1295−1306.
31. Prescott, B., Steinmetz, W., and Thomas, G. J., Jr. (1984) Characterization of DNA structures by laser Raman spectroscopy, *Biopolymers 23*, 235−256.
32. Thomas, G. J., Jr., and Benevides, J. M. (1985) An *A*-helix structure for poly(dA-dT)·poly(dA-dT), *Biopolymers 24*, 1101−1105.
33. Tung, C. S., and Harvey, S. C. (1986) Base sequence, local helix structure, and macroscopic curvature of A-DNA and B-DNA, *J. Biol. Chem. 261*, 3700−3709.
34. Wang, L., Ferrari, M., and Bloomfield, V. A. (1990) Large-scale preparation of mononucleosomal DNA from calf thymus for biophysical studies, *Biotechniques 9*, 24, 26−24, 27.
35. Duguid, J., Bloomfield, V. A., Benevides, J., and Thomas, G. J., Jr. (1993) Raman spectroscopy of DNA−metal complexes. I. Interactions and conformational effects of the divalent cations: Mg, Ca, Sr, Ba, Mn, Co, Ni, Cu, Pd, and Cd, *Biophys. J. 65*, 1916−1928.
36. Overman, S. A., and Thomas, G. J., Jr. (1995) Raman spectroscopy of the filamentous virus Ff (fd, fl, M13): structural interpretation for coat protein aromatics, *Biochemistry 34*, 5440−5451.
37. Tsuboi, M., Benevides, J. M., and Thomas, G. J., Jr. (2004) Structural analysis of drug intercalation: polarized Raman microspectroscopy of the complex between ethidium and genomic DNA, *Biophys. J. 86*, 138a.
38. Thomas, G. J., Jr., Prescott, B., and Olins, D. E. (1977) Secondary structure of histones and DNA in chromatin, *Science 197*, 385−388.
39. Erfurth, S. C., Bond, P. J., and Peticolas, W. L. (1975) Characterization of the A D B transition of DNA in fibers and gels by laser Raman spectroscopy, *Biopolymers 14*, 1245−1257.
40. Duguid, J. G., Bloomfield, V. A., Benevides, J. M., and Thomas, G. J., Jr. (1996) DNA melting investigated by differential scanning calorimetry and Raman spectroscopy, *Biophys. J. 71*, 3350−3360.
41. Serban, D., Benevides, J. M., and Thomas, G. J., Jr. (2002) DNA secondary structure and Raman markers of supercoiling in *Escherichia coli* plasmid pUC19, *Biochemistry 41*, 847−853.
42. Winkle, S. A., Rosenberg, L. S., and Krugh, T. R. (1982) On the cooperative and noncooperative binding of ethidium to DNA, *Nucleic Acids Res. 10*, 8211−8223.
43. Movileanu, L., Benevides, J. M., and Thomas, G. J., Jr. (2002) Determination of base and backbone contributions to the thermodynamics of premelting and melting transitions in *B* DNA, *Nucleic Acids Res. 30*, 3767−3777.
44. Reilly, K. E., and Thomas, G. J., Jr. (1994) Hydrogen exchange dynamics of the P22 virion determined by time-resolved Raman spectroscopy: effects of chromosome packaging on the kinetics of nucleotide exchanges, *J. Mol. Biol. 241*, 68−82.
45. Zama, M., Olins, D. E., Prescott, B., and Thomas, G. J., Jr. (1978) Nucleosome conformation: pH and organic solvent effects, *Nucleic Acids Res. 5*, 3881−3897.
46. Overman, S. A., Aubrey, K. L., Reilly, K. E., Osman, O., Hayes, S. J., Serwer, P., and Thomas, G. J., Jr. (1998) Conformation and interactions of the packaged double-stranded DNA genome of bacteriophage T7, *Biospectroscopy 4*, S47−S56.
47. Thomas, G. J., Jr. (1999) Raman spectroscopy of protein and nucleic acid assemblies, *Annu. Rev. Biophys. Biomol. Struct. 28*, 1−27.
48. Deng, H., Bloomfield, V. A., Benevides, J. M., and Thomas, G. J., Jr. (2000) Structural basis of polyamine-DNA recognition: spermidine and spermine interactions with genomic *B*-DNAs of different GC content probed by Raman spectroscopy, *Nucleic Acids Res. 28*, 3379−3385.
49. Tuma, R., and Thomas, G. J., Jr. (2002) in *Handbook of Vibrational Spectroscopy, Volume 5, Applications in Life, Pharmaceutical and Natural Sciences* (Chalmers, J. M., and Griffiths, P. R., Eds.) pp 3519−3535, John Wiley & Sons, Chichester, U.K.
50. Peticolas, W. L., and Evertsz, E. (1992) Conformation of DNA in vitro and *in vivo* from laser Raman scattering, *Methods Enzymol. 211*, 335−352.
51. Nishimura, Y., Tsuboi, M., Nakano, T., Higuchi, S., Sato, T., Shida, T., Uesugi, S., Ohtsuka, E., and Ikehara, M. (1983) Raman diagnosis of nucleic acid structure: sugar-puckering and glycosidic conformation in the guanosine moiety, *Nucleic Acids Res. 11*, 1579−1588.
52. Benevides, J. M., and Thomas, G. J., Jr. (1983) Characterization of DNA structures by Raman spectroscopy: high-salt and low-salt forms of double helical poly(dG-dC) in H_2O and D_2O solutions and application to *B*, *Z* and *A*-DNA, *Nucleic Acids Res. 11*, 5747−5761.
53. Nishimura, Y., Tsuboi, M., Sato, T., and Aoki, K. (1986) Conformation-sensitive Raman lines of mononucleotides and their use in a structure analysis of polynucleotides: guanine and cytosine nucleotides, *J. Mol. Struct. 146*, 123−153.
54. Dijkstra, S., Benevides, J. M., and Thomas, G. J., Jr. (1991) Solution conformations of nucleoside analogues exhibiting antiviral activity against human immunodeficiency virus, *J. Mol. Struct. 242*, 283−301.
55. Movileanu, L., Benevides, J. M., and Thomas, G. J., Jr. (1999) Temperature dependence of the Raman spectrum of DNA. I. Raman signatures of premelting and melting transitions of poly(dA-dT)·poly(dA-dT), *J. Raman Spectrosc. 30*, 637−649.
56. Movileanu, L., Benevides, J. M., and Thomas, G. J., Jr. (2002) Temperature dependence of the Raman spectrum of DNA. II. Raman signatures of premelting and melting transitions of poly(dA)·poly(dT) and comparison with poly(dA-dT)·poly(dA-dT), *Biopolymers 63*, 181−194.
57. Benevides, J. M., Overman, S. A., and Thomas, G. J., Jr. (2003) in *Current Protocols in Protein Science* (Coligan, J. E., Dunn, B. M., Ploegh, H. L., Speicher, D. W., and Wingfield, P. T., Eds.) pp 17.8.1−17.8.35, John Wiley and Sons, New York.
58. Erfurth, S. C., Kiser, E. J., and Peticolas, W. L. (1972) Determination of the backbone structure of nucleic acids and nucleic acid oligomers by laser Raman scattering, *Proc. Natl. Acad. Sci. U.S.A. 69*, 938−941.
59. Thomas, G. J., Jr., and Hartman, K. A. (1973) Raman studies of nucleic acids. VIII. Estimation of RNA secondary structure from Raman scattering by phosphate group vibrations, *Biochim. Biophys. Acta 312*, 311−322.
60. Small, E. W. and Peticolas, W. L. (1971) Conformational dependence of the Raman scattering intensities from polynucleotides, *Biopolymers 10*, 69−88.
61. Benevides, J. M., Wang, A. H. J., Rich, A., Kyogoku, Y., van der Marel, G. A., van Boom, J. H., and Thomas, G. J., Jr. (1986) Raman spectra of single crystals of r(GCG)d(CGC) and d(CCCCGGGG) as models for *A* DNA, their structure transitions in aqueous solution, and comparison with double-helical poly(dG)·poly(dC), *Biochemistry 25*, 41−50.
62. Katahira, M., Lee, S. J., Kobayashi, Y., Sugeta, H., Kyogoku, Y., Iwai, S., Ohtsuka, E., Benevides, J. M., and Thomas, G. J., Jr. (1990) Structure in solution of the RNA·DNA hybrid $(rA)_8$·$(dT)_8$ determined by NMR and Raman spectroscopy, *J. Am. Chem. Soc. 112*, 4508−4512.
63. Thomas, G. J., Jr., Prescott, B., Opella, S. J., and Day, L. A. (1988) Sugar pucker and phosphodiester conformations in viral genomes of filamentous bacteriophages: fd, If1, IKe, Pf1, Xf, and Pf3, *Biochemistry 27*, 4350−4357.
64. Evertsz, E. M., Thomas, G. A., and Peticolas, W. L. (1991) Raman spectroscopic studies of the DNA cro binding site conformation, free and bound to cro protein, *Biochemistry 30*, 1149−1155.

BI048651L